

Improving Compressed Sensing Image Reconstruction Based on Atmospheric Modulation Using the Distributed Cumulative Synthesis Method

X. Lei ^{1b}, X. Ma ^{1b}, Z. Yang, X. Peng, Y. Li, M. Zhao, and M. Fan

Abstract—The problem of long-distance imaging through time-varying scattering media, such as the atmosphere, is encountered in many science fields. Recent studies have demonstrated that random atmospheric variability can be considered a spatial light modulator in compressed sensing imaging. However, the quality of the reconstructed image needs to be further improved. In this paper, we propose a distributed cumulative synthesis method to improve the compressed sensing image reconstruction based on atmospheric modulation. For multiple original images of various types, the compressed sensing imaging simulation experiment with different sampling rates was conducted using the distributed cumulative synthesis method. The simulation results show that, compared with the imaging method using a single light source, the distributed cumulative synthesis method can effectively improve the quality of the reconstructed image, whether it is full sampling or under-sampling. In addition, a sparsity impact factor is defined to quantify the reconstruction ability of the measurement matrix obtained by the distributed cumulative synthesis method. This value can be used as an evaluation index for the optimized design of the measurement matrix by the distributed cumulative synthesis method. Noise analysis shows that the proposed method has better anti-noise performance than the single light source imaging method.

Index Terms—Atmospheric modulation, compressed sensing, distributed cumulative synthesis, measurement matrix.

I. INTRODUCTION

RANDOM scattering media can cause severe image quality degradation, rendering it difficult to image targets in or hidden behind a scattering medium [1]–[3]. When the scattering effect is weak, the optical coherence and propagation direction are consistent with those of the incident light. Although imaging through the scattering medium can be achieved by extracting ballistic photons [4],[5], the ballistic light intensity decays exponentially as the propagation distance increases, which significantly limits the effective imaging distance. Previous studies

have proved that photons still contain considerable effective information after multiple scattering in the medium [3],[6], which demonstrates that the scattering medium is not the main limitation for imaging. Further, these seemingly random scattered photons also carry some target information. Wavefront shaping [2],[7]–[9] is a method that uses scattering media to achieve focusing and imaging at a desired position. This method requires auxiliary equipment in most cases, which limits its application in practice. Speckle correlation imaging [10]–[12] based on the “memory effect” [13] of the scattering medium has also attracted research interest. The experimental requirements of speckle-related methods are relatively simple, but the imaging field of view is limited by the memory effect range, which is inversely proportional to the medium thickness. With the development of deep learning [14], an increasing number of researchers are using neural networks to address these issues concerning the scattering media problem [15]–[17]. Indeed, deep learning has shown great potential in solving the problems caused by scattering, but it is limited by the training data. Furthermore, the trained network lacks generalizability and flexibility.

Compressed sensing (CS) [18]–[20], which is a new guiding theory for information acquisition, has increasingly gained interest. In 2010, Popoff *et al.* [21],[22] proposed scattering media as promising candidates for designing efficient and compact compressive imagers. This concept eliminates the need to design a measurement matrix because the scattering media that exist in nature can be used as spatial light modulators in CS imaging. Recently, we proposed and verified a CS imaging model based on atmospheric scattering media modulation [23]. To further improve the imaging quality, in this paper, we propose a distributed cumulative synthesis method. In this method, multiple light sources simultaneously emit laser beams to illuminate the same target through an atmospheric scattering medium, and the modulation pattern formed by each light source is accumulated to form a measurement matrix.

The remainder of this paper is organized as follows. In Section II, we present the proposed distributed cumulative synthesis model of atmospheric scattering media modulation based on the theoretical analysis of the impact on CS imaging quality. In Section III, we first prove that the measurement matrices of the distributed cumulative synthesis satisfy the restricted isometry property (RIP) condition of CS. Then, through the results of simulation experiments, we prove that the distributed cumulative synthesis method can effectively improve the imaging quality

Manuscript received July 19, 2021; revised August 23, 2021; accepted August 24, 2021. Date of publication August 30, 2021; date of current version September 15, 2021. This work was supported by the Key Cultivation Foundation of the National Space Science Center, Chinese Academy of Sciences. (Corresponding author: Xiaoshan Ma.)

X. Lei, X. Ma, Z. Yang, X. Peng, Y. Li, M. Zhao, and M. Fan are with the Key Laboratory of Electronics and Information Technology for Space System, National Space Science Center, Chinese Academy of Sciences, Beijing 100190, China. X. Lei, M. Zhao, and M. Fan are also with the University of Chinese Academy of Sciences, Beijing 10049, China (e-mail: leixuelin16@mails.ucas.ac.cn; maxs@nssc.ac.cn; yangzhen@nssc.ac.cn; pxd@nssc.ac.cn; liyunllyyy@sina.com; zhaomengyuan17@mails.ucas.ac.cn; fanmingrui17@mails.ucas.ac.cn).

Digital Object Identifier 10.1109/JPHOT.2021.3108194

compared with a single light source. In Section IV, we define the sparsity impact factor to quantitatively analyze the ability of the measurement matrix to reconstruct the image. Different degrees of noise analysis simulation experiments demonstrate that the distributed cumulative synthesis method has better anti-noise ability. Finally, in Section V, we summarize the study and its main results.

II. METHODS

A. Theoretical Analysis

According to CS theory, if a signal is sparse, it can be reconstructed from several samples [24]. In addition, the CS sampling rate is much lower than the Nyquist sampling rate. The CS technique is divided into two processes: sampling and reconstruction. In the sampling process, the original signal is linearly projected into a low-dimensional space through a specific measurement matrix. The original signal can then be recovered using the prior information of the signal and the reconstruction algorithm, which is the reconstruction process. Assuming that x is a signal of length N , there is a sparse basis Ψ such that $x = \Psi s$. Then s is the sparse vector of the signal x projected on the sparse basis Ψ . If there are I ($I \ll N$) coefficients with large values in vector s , and most other coefficients are close to or equal to zero, then this signifies that the signal can be compressed. A matrix Φ that is not related to the sparse basis Ψ is used to compress x , and the sampling model is expressed as

$$y = \Phi x = \Phi (\Psi s) = (\Phi \Psi) s = \Theta s, \quad (1)$$

where y is the measured value and Φ is the $M \times N$ ($M \leq N$) measurement matrix. M is the number of samples. The product of Φ and Ψ provides an $M \times N$ matrix, Θ .

In a previous work, we have demonstrated that the randomness of atmospheric scattering media can be used as an instantaneous compression imaging mechanism [23]. When a laser beam passes through the atmospheric scattering medium, the scattering medium will modulate the light field to obtain a series of stochastic and time-varying modulation patterns. If a target of interest is illuminated with these modulation patterns and a bucket detector is used to collect data from the target, the CS imaging can be realized. Using the measurement matrix formed by the modulation patterns and the measurement values from the detector, the target information can be recovered by CS reconstruction algorithm. The modulation effect of the atmosphere can be described by the atmospheric point spread function (PSF). Given the surface meteorological range and atmospheric optical thickness, the PSF can be simulated by the backward Monte Carlo (MC) [25],[26] algorithm. The PSF obtained is a single modulation pattern Φ_m ($m = 1, 2, \dots, M$) in CS. Its expression is as follows:

$$\Phi_m = \begin{bmatrix} a_{11}^m & \cdots & a_{1n}^m \\ \vdots & \ddots & \vdots \\ a_{n1}^m & \cdots & a_{nn}^m \end{bmatrix} \quad (2)$$

where a represents an element in the matrix of PSF. The size of the modulation pattern Φ_m is $n \times n$, which is the same as the size of the image to be reconstructed. Each pattern is stretched into a row vector as a row of the measurement matrix,

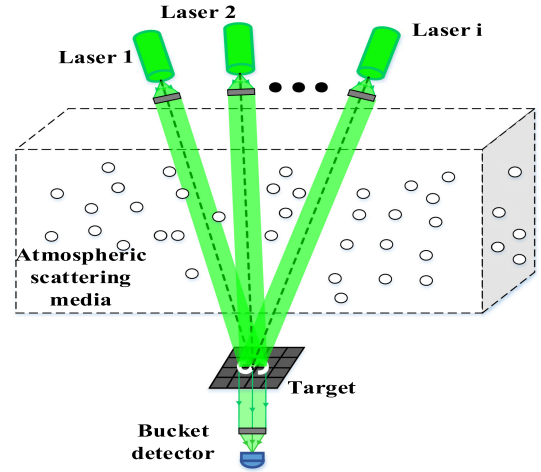


Fig. 1. Schematic of the distributed cumulative synthesis modulation imaging based model. Multiple laser beams enter the atmosphere from different directions and illuminate the same target after modulation by the atmospheric scattering media.

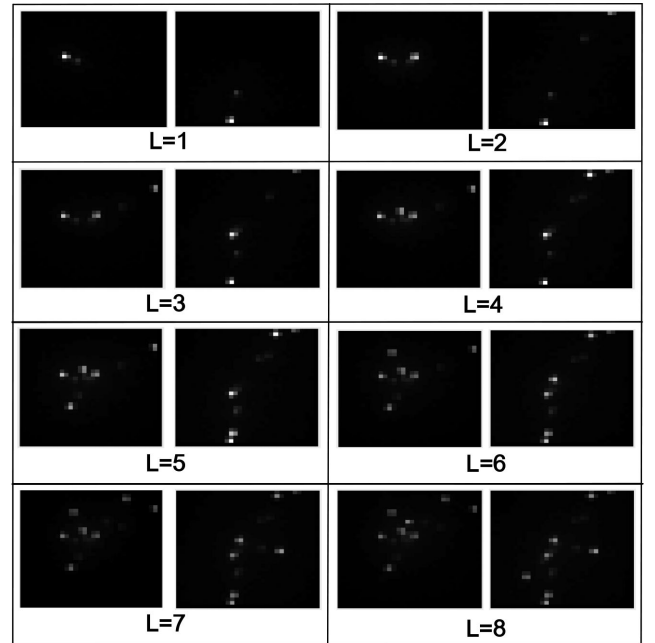


Fig. 2. Examples of two sets of cumulative modulation patterns produced by different numbers of laser sources L ($L = 1-8$). L is increased from 1 to 8. The pixel size of the modulation pattern is 32×32 .

and multiple modulation patterns can form the measurement matrix Φ . The previously proposed CS imaging model was based on atmospheric modulation with only one light source, and the single modulation pattern Φ_m is shown in Fig. 2 ($L = 1$).

When reconstructing the image with CS, to ensure that sufficient information can be collected, the sampling corresponding to the measurement matrix must cover every dimension of the original signal [27]. That is, every column of the measurement matrix must have at least one non-zero value, to ensure that the data of the signal corresponding to the column is collected. The coverage of the measurement matrix (CMM) [27]–[29] is defined as the proportion of the number of non-zero columns to

the total number of columns. Its expression is as follows:

$$CMM = 1 - \left(\frac{N - K}{N} \right)^M \quad (3)$$

where N is the number of columns of the measurement matrix. K is the sparsity of a single modulation pattern Φ_m . To ensure that the measurement matrix collects all the information of the original signal, the CMM should be close to one. However, in different practical applications, the length N of the original signal is changed. Therefore, we use the number of zero columns of the measurement matrix (N_{ZC}) to satisfy $N_{ZC} < 1$ as the condition of CMM (condition 1). The condition can be expressed as follows:

$$N_{ZC} = (1 - CMM) \times N = \left(\frac{N - K}{N} \right)^M \times N < 1 \quad (4)$$

The CMM condition (condition 1) of (4) shows that the larger the value of the sparsity K , the more complete the sampled information and the higher the quality of the target reconstruction.

However, other studies have shown that the smaller the sparsity K value of a single modulation pattern Φ_m , the better the quality of the reconstructed image (condition 2) [30]. This is because, when the sparsity value of the single modulation pattern is small, the interference between pixels in the image is reduced. At the same time, the sparse measurement can more clearly reflect the sparsity of the signal itself, which is more conducive to the CS algorithm resolving the signal.

Therefore, the sparsity of a single modulation pattern Φ_m of the measurement matrix is restricted by the above two conditions. The optimal value of sparsity is the smallest value that satisfies the CMM condition. For example, to reconstruct a 32×32 pixel image with full sampling ($M = 1024$), the value range of the sparsity calculated according to condition 1 is as follows: $K > 6.91$. K must be a positive integer, thus, the value range of K is as follows: $K > 7$. Condition 2 indicates that the value of the sparsity K should be minimized. Therefore, for comprehensively analyzing conditions 1 and 2, the optimal sparsity value of a single modulation pattern Φ_m is seven.

The above analysis shows that there is an optimal sparsity value for a single modulation pattern. To achieve high-quality image reconstruction, the modulation pattern needs to be optimized to achieve the optimal sparsity value. When all the modulation patterns reach the optimal sparsity value, the composed measurement matrix is optimal. In fact, it is difficult to ensure that all modulation patterns attain the optimal sparsity value, however, a higher number of modulation patterns attaining the optimal sparsity value indicates a better-quality image reconstruction by the measurement matrix. Taking this as the basis, this study aims to optimize the measurement matrix through the distributed cumulative synthesis method, thereby improving the quality of image reconstruction.

B. Distributed Cumulative Synthesis Model Based on Atmospheric Modulation

The above theoretical analysis indicates that there is an optimal sparsity value for a single modulation pattern in the CS model based on atmospheric modulation. The greater the number of modulation patterns of the optimal sparsity value, the better

the image quality of the measurement matrix reconstruction. When the pixel size of the reconstructed image is 32×32 , the optimal sparsity value of a single modulation pattern Φ_m is seven. Fig. 2 ($L = 1$) shows that when only one light source illuminates the atmospheric scattering medium, the sparsity value of a single modulation pattern Φ_m is evidently less than seven. To improve the quality of CS imaging based on atmospheric modulation, we propose a distributed cumulative synthesis method to increase the sparsity value of Φ_m . The model is shown in Fig. 1. Multiple laser light sources pass through the atmosphere in different directions, and each light field formed by the modulation of the atmospheric scattering medium is accumulated to form a total modulated light field. The modulated light passes through the transmission target and is finally collected by the barrel detector. The mathematical expression of the modulation pattern Φ_m^L ($m = 1, 2, \dots, M$) obtained by the distributed cumulative synthesis method is as follows:

$$\Phi_m^L = \sum_{i=1}^{i=L} \Phi_{mi} = \sum_{i=1}^{i=L} \begin{bmatrix} a_{11}^{mi} & \cdots & a_{1n}^{mi} \\ \vdots & \ddots & \vdots \\ a_{n1}^{mi} & \cdots & a_{nn}^{mi} \end{bmatrix} \quad (5)$$

where matrix Φ_m^L is the total modulation pattern obtained by the distributed cumulative synthesis method, and Φ_{mi} represents the m -th modulation pattern obtained when the i -th light source is illuminated. L is the total number of light sources.

Examples of Φ_m^L are shown in Fig. 2; the pixel size of the reconstructed image is 32×32 . These images show that as the number of laser light sources increases, the gray value of the modulation pattern is accumulated pixel by pixel, and the distribution range with high gray values gradually increases. As a result, the value of the sparsity of the modulation pattern Φ_m^L is increased, the collected target information is sufficient, and the quality of the reconstructed image is improved. After obtaining a single modulation pattern Φ_m^L , 1024 modulation patterns are simulated by randomly changing the transmission direction. These patterns are used to generate a measurement matrix that meets all sampling requirements. The generation process can also be expressed by a mathematical formula. Assuming that the size is $n \times n$ and the modulation pattern Φ_m^L is

$$\Phi_m^L = \sum_{i=1}^{i=L} \begin{bmatrix} a_{11}^{mi} & \cdots & a_{1n}^{mi} \\ \vdots & \ddots & \vdots \\ a_{n1}^{mi} & \cdots & a_{nn}^{mi} \end{bmatrix} = \begin{bmatrix} a_{11}^m & \cdots & a_{1n}^m \\ \vdots & \ddots & \vdots \\ a_{n1}^m & \cdots & a_{nn}^m \end{bmatrix} \quad (6)$$

a single modulation pattern is stretched into a row vector as a row of the measurement matrix, the combined measurement matrix Φ is follows:

$$\Phi = \begin{bmatrix} a_{11}^1 & \cdots & a_{1n}^1 & a_{21}^1 & \cdots & a_{nn}^1 \\ a_{11}^2 & \cdots & a_{1n}^2 & a_{21}^2 & \cdots & a_{nn}^2 \\ \vdots & \vdots & \vdots & \vdots & \vdots & \vdots \\ a_{11}^m & \cdots & a_{1n}^m & a_{21}^m & \cdots & a_{nn}^m \\ \vdots & \vdots & \vdots & \vdots & \vdots & \vdots \\ a_{11}^{M-1} & \cdots & a_{1n}^{M-1} & a_{21}^{M-1} & \cdots & a_{nn}^{M-1} \\ a_{11}^M & \cdots & a_{1n}^M & a_{21}^M & \cdots & a_{nn}^M \end{bmatrix} \quad (7)$$

where M is the number of samples, that is, the number of rows of the measurement matrix Φ .

TABLE I
AVERAGE CORRELATION COEFFICIENTS BETWEEN THE FOURIER SPARSE BASIS
AND THE MEASUREMENT MATRIX OF THE DISTRIBUTED CUMULATIVE
SYNTHESIS METHOD

Number of lasers	1	2	3	4	5	6	7	8
μ_{ave}	0.0056	0.0067	0.0058	0.0049	0.0054	0.0053	0.0054	0.0065

III. RESULTS

A. RIP

The measurement matrix construction is known to directly affect the sampling accuracy of the CS technique. In this context, Candes *et al.* [31] proposed the RIP of the measurement matrix, whereby the matrix satisfying the RIP can be used as a measurement matrix to achieve good reconstruction. However, in practice, it is difficult to assess whether a matrix satisfies the RIP condition and to use the RIP to guide the design of the measurement matrix. Donoho and Elad [32] subsequently proposed that a weaker coherence between the measurement and sparse matrices indicates a greater probability of the measurement matrix satisfying the RIP condition. Based on this, several indicators [33]–[35] were proposed to measure this correlation, including the maximum correlation coefficient, average correlation coefficient, cumulative correlation coefficient, and power average correlation coefficient. Among them, the average correlation coefficient μ_{ave} represents the overall correlation of the measurement matrix, and its definition is as follows:

$$\mu_{ave} \{ \Phi, \Psi \} = \frac{\sum_{1 \leq i, j \leq N} \{ \langle \varphi_i, \psi_j \rangle \}}{N(N-1)}, \quad (8)$$

where Φ and Ψ are the measurement and sparse matrices, respectively.

To investigate whether the measurement matrix obtained by the distributed cumulative synthesis method satisfies the uncorrelated condition, the average correlation coefficients were computed, as listed in Table I. In the calculation process, we chose the commonly used Fourier matrix as the sparse base. As indicated, the calculated correlation coefficients are small; therefore, they satisfy the uncorrelated condition. That is, the measurement matrices obtained by the distributed cumulative synthesis method (the number of light sources is increased from 1 to 8) meet the RIP for CS.

B. Simulation Experiment

We then employed the measurement matrices obtained via distributed cumulative synthesis to perform a CS imaging simulation experiment. The imaging process shown in Fig. 3 includes measurement value acquisition and original image reconstruction. The modulation effect of the atmosphere is first obtained by MC simulation. Then, the measurement matrix is obtained by the distributed cumulative synthesis method. According to the sampling principle of CS, the measured values can be obtained by multiplying the measurement matrix and the selected original image. This is the process of obtaining the measured values. Subsequently, the measured values are used as input to the

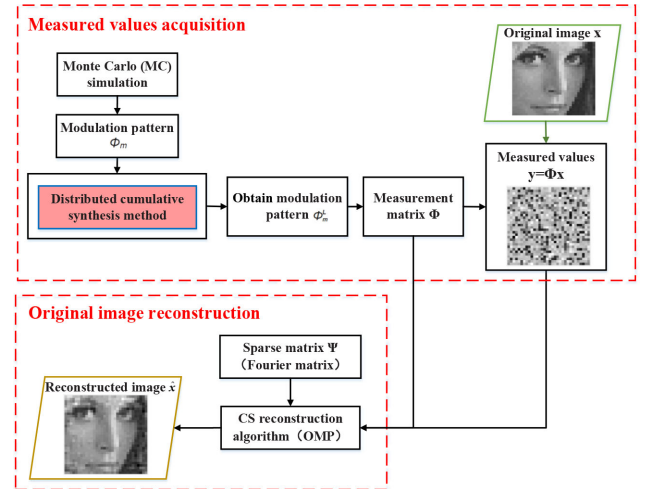


Fig. 3. Imaging process of the CS experiment.

original image	L=1	L=2	L=3	L=4	L=5	L=6	L=7	L=8
GIRL								
	24.5305	27.6203	27.7040	28.9769	28.7215	28.7518	28.3093	27.3212
BRAIN								
	16.9757	18.8690	19.3058	20.5744	20.1831	19.6474	19.3485	19.4028
HOUSE								
	19.6108	21.7602	22.2596	22.9974	22.5384	23.1033	21.2859	22.0455

Fig. 4. Image reconstruction results of simulation experiments.

CS reconstruction algorithm to recover the target image. The reconstruction algorithm used here is an orthogonal matching pursuit (OMP) algorithm, and the sparse matrix is a Fourier matrix.

The effectiveness of the distributed cumulative synthesis method is demonstrated by determining the similarities between the original and reconstructed target images. The peak signal-to-noise ratio (PSNR) is an objective criterion for evaluating image quality; it is defined as

$$PSNR = 10 \log_{10} \left(\frac{1}{\sum_{i=1}^N (x_i - \hat{x}_i)^2 / N} \right) \quad (9)$$

where x_i and \hat{x}_i represent the original and reconstructed images, respectively, and N is the total number of pixels.

We chose three different original images (Fig. 4) as the simulation experiment targets. The image labeled GIRL is a screenshot of a person's facial expression, whereas the BRAIN image shows a magnetic resonance imaging (MRI) scan of the brain. The last picture, named HOUSE, is an image of a house. The size of each target image is 32×32 pixels. The results of the simulation experiment are shown in Fig. 4. The sampling method was full sampling. The PSNR values show that, compared with a single light source, the use of distributed cumulative synthesis improves the quality of CS reconstructed images. The images labeled GIRL and BRAIN exhibit the best reconstructed image quality when the number of lasers is four ($i = 4$), while the image labeled HOUSE yields the best image quality when the number of lasers is six ($i = 6$).

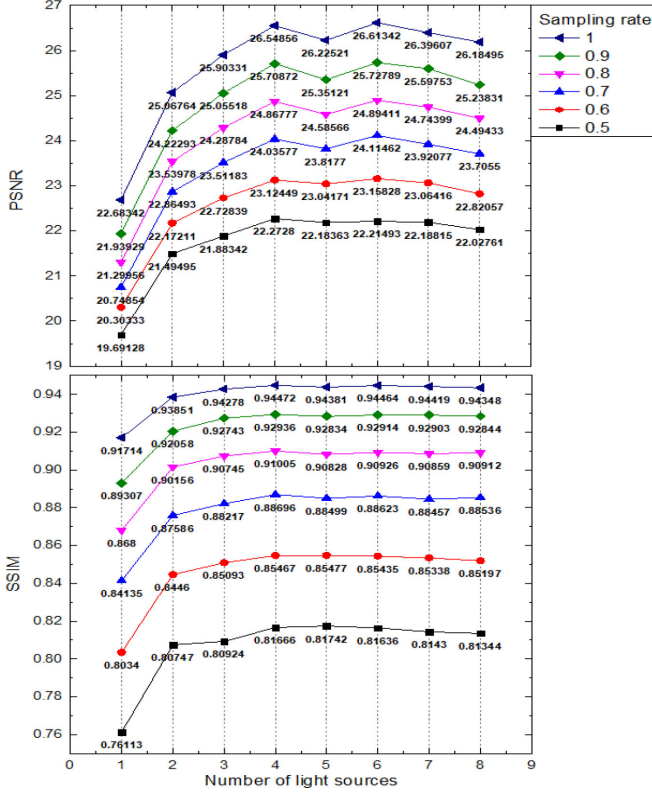


Fig. 5. Statistics of the simulation results obtained using 300 randomly selected original images. The abscissa denotes the number of distributed lasers used to synthesize the atmospheric modulation matrix. The y-axis represents the PSNR and SSIM of the reconstructed image.

These simulation results demonstrate that different targets can affect the reconstruction quality. Therefore, we conducted numerous simulation experiments for different target images and performed a statistical analysis of the results. We randomly selected 300 original images at 32×32 pixels. These 300 pictures—100 pictures of human faces, 100 MRI scan images, and 100 architectural images—were obtained from the internet. To comprehensively measure the quality of the reconstructed images, structural similarity image measurement (SSIM) is added as another criterion. Its mathematical expression is as follows:

$$SSIM(x_i, \hat{x}_i) = \frac{(2\mu_{x_i}\mu_{\hat{x}_i} + C_1)(2\delta_{x_i\hat{x}_i} + C_2)}{(\mu_{x_i}^2 + \mu_{\hat{x}_i}^2 + C_1)(\delta_{x_i}^2 + \delta_{\hat{x}_i}^2 + C_2)} \quad (10)$$

where x_i and \hat{x}_i represent the original and reconstructed images, respectively. μ_{x_i} and $\mu_{\hat{x}_i}$ represent the mean values of images x_i and \hat{x}_i , δ_{x_i} and $\delta_{\hat{x}_i}$ represent the variances of images x_i and \hat{x}_i , and $\delta_{x_i\hat{x}_i}$ represents the covariance of images x_i and \hat{x}_i . C_1 and C_2 are taken as constants to prevent the denominator from being equal to zero. The statistical results of the simulation experiment (the average values of PSNR and SSIM) are depicted in Fig. 5. The x -axis presents the number of lasers for distributed cumulative synthesis. The M to N ratio in (1) is defined as the sampling rate, and its range of values is 0.5 to 1 (shown by different colors and symbols in Fig. 5). The statistical results of multiple simulation experiments show that when the number of accumulated light sources is greater than one, the quality

of the reconstructed image is significantly improved, which further confirms the effectiveness of the distributed cumulative synthesis method.

IV. DISCUSSION

A. Sparsity Impact Factor

Based on the theoretical analysis of the optimal sparsity of the modulation pattern in Section II, a quantitative study on the reconstruction ability of the measurement matrix obtained by the distributed cumulative synthesis method was carried out. According to conditions 1 and 2, it can be confirmed that the single modulation pattern has an optimal sparsity value.

The quality of the target image reconstructed by the measurement matrix increases with the number of modulation patterns with optimal sparsity in the measurement matrix. In Fig. 5, the target image size is 32×32 pixels and the number of lasers used to illuminate the target ranges from one to eight. For a given illumination setup, under full sampling conditions, there are 1024 synthetic atmospheric modulation patterns Φ_m^L to constitute the measurement matrix Φ for the CS technique. To measure the overall impact of the sparsity of these 1024 modulation patterns on the quality of the reconstructed image, we set a sparsity impact factor calculation formula as follows:

$$IF_{sparsity} = 0.4 \times Q_4 + 0.6 \times Q_5 + 0.8 \times Q_6 + 1 \times Q_7 + 0.8 \times Q_8 + 0.6 \times Q_9 + 0.4 \times Q_{10} \quad (11)$$

where Q_n denotes the number of modulation patterns among the 1024 modulation patterns whose sparseness is n . For example, Q_4 denotes the number of modulation patterns whose sparseness is four. The weights 0.4, 0.6, 0.8, and 1 are determined according to the difference in the optimal sparsity. Because the optimal sparsity is seven for a target image with a size of 32×32 pixels, Q_7 has the highest weight. However, in the simulation, the element value of the atmospheric modulation pattern is between zero and one (grayscale modulation). Therefore, to obtain the sparsity of the modulation pattern, all elements of the matrix must be binarized. We set the top 80% elements of the modulation mode Φ_m^L to one and set the other elements to zero for binarization. The sum of all non-zero values is the sparseness of the modulation pattern.

To make the result more intuitive, it is necessary to normalize the calculated sparsity impact factor. In the best case, i.e., when the sparsity of all modulation patterns Φ_m^L is seven, the value of the impact factor is 1024. Therefore, the normalization method involves the division of the calculated impact factors by 1024. For the normalized sparsity impact factor, the closer the value of the impact factor of the measurement matrix is to one, the better the reconstruction ability of the measurement matrix.

A comparison between the sparsity impact factor value and the reconstructed image quality is shown in Fig. 6. In the figure, the abscissa is the number of distributed lasers needed to synthesize the atmospheric modulation matrix. The y-axes represents the normalized sparsity impact factor value (bottom), SSIM (middle) and PSNR (top) of the reconstructed image. The figure shows that there is good consistency between the

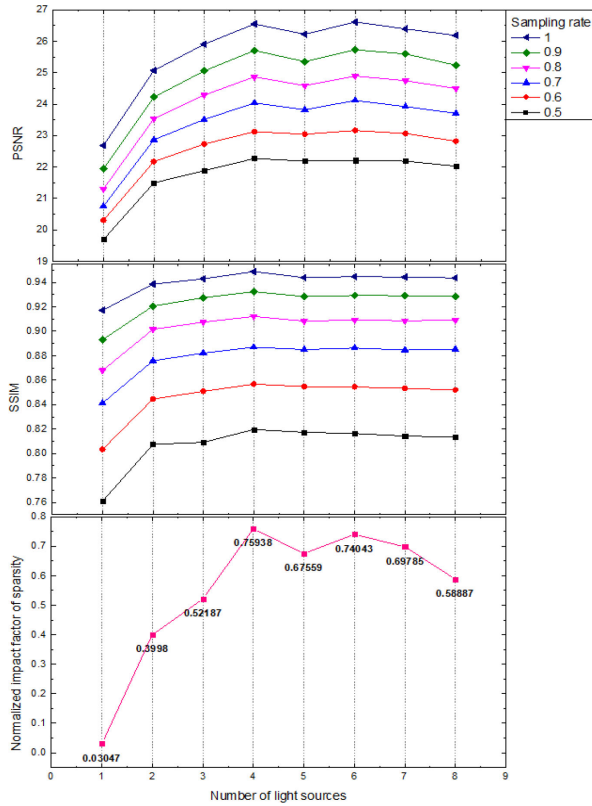


Fig. 6. Comparison between normalized sparsity impact factor value and reconstructed image quality for different numbers of lasers. The abscissa denotes the number of distributed lasers used to synthesize the atmospheric modulation matrix. The y-axes represents the normalized sparsity impact factor value (bottom), SSIM (middle) and PSNR (top) of the reconstructed image.

normalized sparsity impact factor of the measurement matrix and the quality of the reconstructed image. When the number of light sources increases from one to four, the normalized sparsity impact factor of the measurement matrix increases, indicating that the reconstruction ability of the measurement matrix obtained by increasing the number of light sources is gradually enhanced. A further increase in the number of light sources does not result in an increase in the normalized sparsity impact factor of the measurement matrix, implying the quality of image reconstruction will not improve any further. This result shows that the distributed cumulative synthesis method has a better image reconstruction ability than the single light source method, which is consistent with the theoretical analysis. This sparsity impact factor can be used as an evaluation index to optimize the measurement matrix by the distributed cumulative synthesis method.

B. Noise Analysis

In the process of image reconstruction, noise is inevitable. To further illustrate the effectiveness of the distributed cumulative synthesis method, we investigated noise. The signal-to-noise ratio is generally used to measure the size of the noise; its mathematical formula is as follows:

$$SNR_{dB} = 10 \log_{10} \left(\frac{P_{signal}}{P_{noise}} \right) \quad (12)$$

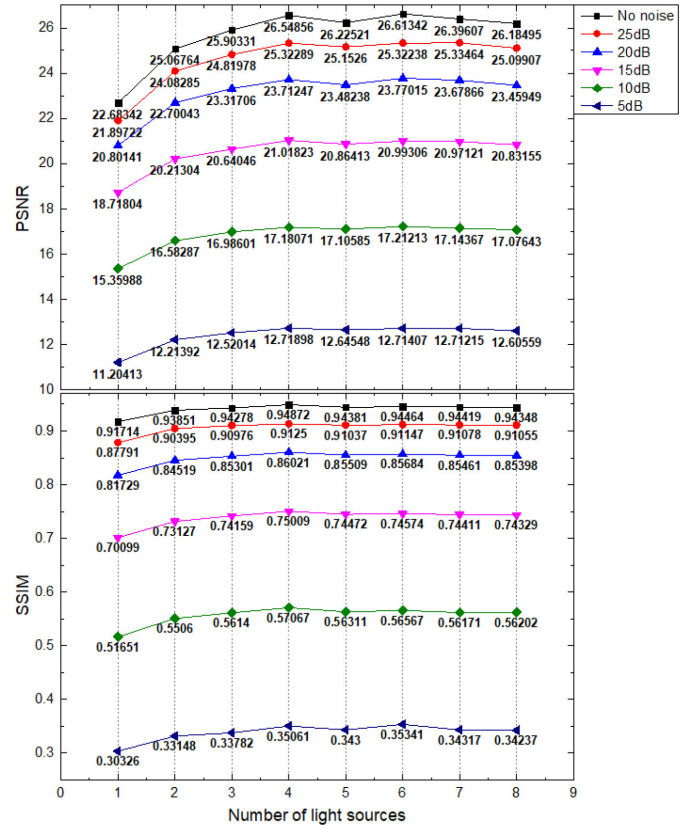


Fig. 7. Experimental results of noise analysis of 300 images based on the method of distributed cumulative synthesis. The abscissa denotes the number of distributed lasers used to synthesize the atmospheric modulation matrix. The y-axis represents the PSNR and SSIM of the reconstructed image.

where P_{signal} and P_{noise} represent the power of the signal and the power of the noise, respectively. The Gaussian noise with a signal-to-noise ratio of 5 dB to 25 dB is selected and added to the measured value in the CS imaging simulation experiment. The OMP algorithm is used to reconstruct the target image in the presence of noise. The experimental results of noise analysis on 300 images based on the distributed cumulative synthesis method are shown in Fig. 7. As the intensity of the added noise gradually increases, the overall quality of the reconstructed image decreases. With the same noise interference, the quality of the image reconstructed by the distributed cumulative synthesis method is better. This shows that the distributed cumulative synthesis method has better anti-noise performance than the single light source method.

V. CONCLUSION

In this paper, we proposed a distributed cumulative synthesis method to improve the quality of CS imaging based on atmospheric scattering media modulation. The measurement matrices obtained with the proposed method satisfy the RIP conditions of CS. The simulation experimental results show that the method can effectively improve the imaging quality compared with that obtained using only one light source. The sparsity impact factor is defined to express the reconstruction ability of the measurement matrix. This value shows good consistency with PSNR,

which represents the quality of the reconstructed target image; therefore, it can be chosen as an evaluation index for optimizing the measurement matrix by the distributed cumulative synthesis method. The experimental results based on different degrees of noise show that the proposed distributed cumulative synthesis method has a better anti-noise performance than the single light source method.

However, challenges remain for the realistic application of our proposed method. Adding a laser light source increases the corresponding workload. Moreover, the modulation pattern simulated by the MC method differs from the actual atmospheric modulation. The reason is that different transmission paths and atmospheric conditions cause the modulation patterns obtained by theoretical simulations and actual measurements to differ. This disparity will be investigated in future work and the results presented in due course.

REFERENCES

- [1] J. Aulbach, B. Gjonaj, P. M. Johnson, A. P. Mosk, and A. Legendijk, "Control of light transmission through opaque scattering media in space and time," *Phys. Rev. Lett.*, vol. 106, no. 10, 2011, Art. no. 103901, doi: [10.1103/PhysRevLett.106.103901](https://doi.org/10.1103/PhysRevLett.106.103901).
- [2] S. Rotter and S. Gigan, "Light fields in complex media: Mesoscopic scattering meets wave control," *Rev. Modern Phys.*, vol. 89, no. 1, 2017, doi: [10.1103/RevModPhys.89.015005](https://doi.org/10.1103/RevModPhys.89.015005).
- [3] O. Tzang, A. M. Caravaca-Aguirre, K. Wagner, and R. Piestun, "Adaptive wavefront shaping for controlling nonlinear multimode interactions in optical fibres," *Nature Photon.*, vol. 12, no. 6, pp. 368–374, 2018, doi: [10.1038/s41566-018-0167-7](https://doi.org/10.1038/s41566-018-0167-7).
- [4] S. Sudarsanam, J. Mathew, S. Panigrahi, J. Fade, M. Alouini, and H. Ramchandran, "Real-time imaging through strongly scattering media: Seeing through turbid media, instantly," *Sci. Rep.*, vol. 6, 2016, Art. no. 25033, doi: [10.1038/srep25033](https://doi.org/10.1038/srep25033).
- [5] J. Guan, Y. Cheng, and G. Chang, "Time-domain polarization difference imaging of objects in turbid water," *Opt. Commun.*, vol. 391, pp. 82–87, 2017, doi: [10.1016/j.optcom.2017.01.012](https://doi.org/10.1016/j.optcom.2017.01.012).
- [6] Z. Yaqoob, D. Psaltis, M. S. Feld, and C. H. Yang, "Optical phase conjugation for turbidity suppression in biological samples," *Nature Photon.*, vol. 2, no. 2, pp. 110–115, 2008, doi: [10.1038/nphoton.2007.297](https://doi.org/10.1038/nphoton.2007.297).
- [7] A. Sanjeev, Y. Kapellner, N. Shabairou, E. Gur, M. Sinvani, and Z. Zalevsky, "Non-invasive imaging through scattering medium by using a reverse response wavefront shaping technique," *Sci. Rep.*, vol. 9, no. 1, 2019, Art. no. 12275, doi: [10.1038/s41598-019-48788-9](https://doi.org/10.1038/s41598-019-48788-9).
- [8] M. Zhao, H. Wang, and Z. M. Tian, "Wavefront-shaping-based pattern regeneration through the scattering medium," *J. Opt. Soc. Amer. A*, vol. 36, no. 9, pp. 1483–1487, 2019, doi: [10.1364/JOSAA.36.001483](https://doi.org/10.1364/JOSAA.36.001483).
- [9] S. Jeong, Y. R. Lee, W. Choi, S. Kang, J. H. Hong, J. S. Park, Y. S. Lim, H. G. Park, and W. Choi, "Focusing of light energy inside a scattering medium by controlling the time-gated multiple light scattering," *Nature Photon.*, vol. 12, no. 5, pp. 277–283, 2018, doi: [10.1038/s41566-018-0120-9](https://doi.org/10.1038/s41566-018-0120-9).
- [10] W. S. Tang *et al.*, "Single-shot coherent power-spectrum imaging of objects hidden by opaque scattering media," *Appl. Opt.*, vol. 58, no. 4, pp. 1033–1039, 2019, doi: [10.1364/AO.58.001033](https://doi.org/10.1364/AO.58.001033).
- [11] H. W. Ruan, Y. Liu, J. Xu, Y. J. Huang, and C. H. Yang, "Fluorescence imaging through dynamic scattering media with speckle-encoded ultrasound-modulated light correlation," *Nature Photon.*, vol. 14, no. 8, pp. 511–516, 2020, doi: [10.1038/s41566-020-0630-0](https://doi.org/10.1038/s41566-020-0630-0).
- [12] Y. Baek, K. Lee, J. Oh, and Y. Park, "Speckle-correlation scattering matrix approaches for imaging and sensing through turbidity," *Sensors*, vol. 20, no. 11, pp. 3147, 2020, doi: [10.3390/s20113147](https://doi.org/10.3390/s20113147).
- [13] I. Freund, M. Rosenbluh, and S. Feng, "Memory effects in propagation of optical waves through disordered media," *Phys. Rev. Lett.*, vol. 61, no. 20, pp. 2328–2331, 1988, doi: [10.1103/PhysRevLett.61.2328](https://doi.org/10.1103/PhysRevLett.61.2328).
- [14] Y. LeCun, Y. Bengio, and G. Hinton, "Deep learning," *Nature*, vol. 521, no. 7553, pp. 436–444, 2015, doi: [10.1038/nature14539](https://doi.org/10.1038/nature14539).
- [15] S. Li, M. Deng, J. Lee, A. Sinha, and G. Barbastathis, "Imaging through glass diffusers using densely connected convolutional networks," *Optica*, vol. 5, no. 7, pp. 803–813, 2018, doi: [10.1364/OPTICA.5.000803](https://doi.org/10.1364/OPTICA.5.000803).
- [16] M. Lyu, H. Wang, G. Li, S. Zheng, and G. Situ, "Learning-based lensless imaging through optically thick scattering media," *Adv. Photon.*, vol. 1, no. 3, 2019, doi: [10.1117/1.AP.1.3.036002](https://doi.org/10.1117/1.AP.1.3.036002).
- [17] Q. Li, J. Zhao, Y. Zhang, X. Lai, Z. Chen, and J. Pu, "Imaging reconstruction through strongly scattering media by using convolutional neural networks," *Opt. Commun.*, vol. 477, 2020, doi: [10.1016/j.optcom.2020.126341](https://doi.org/10.1016/j.optcom.2020.126341).
- [18] D. L. Donoho, "Compressed sensing," *IEEE Trans. Inf. Theory*, vol. 52, no. 4, pp. 1289–1306, Apr. 2006, doi: [10.1109/TIT.2006.871582](https://doi.org/10.1109/TIT.2006.871582).
- [19] E. J. Candes, J. Romberg, and T. Tao, "Robust uncertainty principles: Exact signal reconstruction from highly incomplete frequency information," *IEEE Trans. Inf. Theory*, vol. 52, no. 2, pp. 489–509, Feb. 2006, doi: [10.1109/TIT.2005.862083](https://doi.org/10.1109/TIT.2005.862083).
- [20] M. Mangia, F. Pareschi, R. Rovatti, and G. Setti, "Adapted compressed sensing: A game worth playing," *IEEE Circuits Syst. Mag.*, vol. 20, no. 1, pp. 40–60, Firstquarter 2020, doi: [10.1109/MCAS.2019.2961727](https://doi.org/10.1109/MCAS.2019.2961727).
- [21] S. M. Popoff, G. Lerosey, R. Carminati, M. Fink, A. C. Boccarda, and S. Gigan, "Measuring the transmission matrix in optics: An approach to the study and control of light propagation in disordered media," *Phys. Rev. Lett.*, vol. 104, no. 10, 2010, doi: [10.1103/PhysRevLett.104.100601](https://doi.org/10.1103/PhysRevLett.104.100601).
- [22] A. Liutkus *et al.*, "Imaging with nature: Compressive imaging using a multiply scattering medium," *Sci. Rep.*, vol. 4, pp. 5552, 2014, doi: [10.1038/srep05552](https://doi.org/10.1038/srep05552).
- [23] X. Lei, X. Ma, Z. Yang, X. Peng, Y. Li, and W. Ni, "Compressive sensing imaging based on modulation of atmospheric scattering medium," *Appl. Sci.*, vol. 10, no. 13, pp. 4466, 2020, doi: [10.3390/app10134466](https://doi.org/10.3390/app10134466).
- [24] B. Gao, W. L. Woo, Y. He, and G. Y. Tian, "Unsupervised sparse pattern diagnostic of defects with inductive thermography imaging system," *IEEE Trans. Ind. Inform.*, vol. 12, no. 1, pp. 371–383, Feb. 2016, doi: [10.1109/TII.2015.2492925](https://doi.org/10.1109/TII.2015.2492925).
- [25] P. N. Reinersman and K. L. Carder, "Monte Carlo simulation of the atmospheric point-spread function with an application to correction for the adjacency effect," *Appl. Opt.*, vol. 34, no. 21, pp. 4453–4471, 1995, doi: [10.1364/AO.34.004453](https://doi.org/10.1364/AO.34.004453).
- [26] X. S. Ma, H. D. Wang, L. G. Li, Z. Yang, and X. Meng, "Neural network simulation of the atmospheric point spread function for the adjacency effect research," in *Optics in Atmospheric Propagation and Adaptive Systems*, K. U. S. Xix and J. D. Gonglewski, Eds. Bellingham, WA, USA: SPIE-the International Society for Optical Engineering, 2016.
- [27] L. L. Zhen, Y. X. Ri, L. X. Feng, Y. W. Kai, and Z. G. Jie, "Super-resolution ghost imaging via compressed sensing," *Acta Physica Sinica*, vol. 63, no. 22, p. 7, 2014.
- [28] X. ChangBin, Y. XuRi, L. LongZhen, L. XueFeng, Y. WenKai, G. XiaoYong, Z. GuangJie, and Z. Qing, "Sub-Rayleigh imaging via under-sampling scanning based on sparsity constraints," *Chin. Phys. B*, vol. 60, pp. 218–222, 2017.
- [29] L. L. Zhen, "Research on Super-resolution ghost imaging based on sparse measurement," M.S. thesis, Nat. Space Sci. Center, Chin. Acad. Sciences, Beijing, China, 2015.
- [30] C. M. L. E. W. Hui and S. X. G. W. H. Shensheng, "Ghost imaging based on sparse array pseudothermal light system," *Acta Optica Sinica*, vol. 32, no. 5, 2012, Art. no. 0503001, doi: [10.3788/AOS201232.0503001](https://doi.org/10.3788/AOS201232.0503001).
- [31] E. J. Candes, "The restricted isometry property and its implications for compressed sensing," *Comptes Rendus Mathematique*, vol. 346, no. 9–10, pp. 589–592, 2008, doi: [10.1016/j.crma.2008.03.014](https://doi.org/10.1016/j.crma.2008.03.014).
- [32] D. L. Donoho and M. Elad, "Optimally sparse representation in general (nonorthogonal) dictionaries via l_1 minimization," *Proc. Nat. Acad. Sci. United States Amer.*, vol. 100, no. 5, pp. 2197–2202, 2003, doi: [10.1073/pnas.0437847100](https://doi.org/10.1073/pnas.0437847100).
- [33] C. Lu, H. Li, and Z. Lin, "Optimized projections for compressed sensing via direct mutual coherence minimization," *Signal Process.*, vol. 151, pp. 45–55, 2018, doi: [10.1016/j.sigpro.2018.04.020](https://doi.org/10.1016/j.sigpro.2018.04.020).
- [34] C. Tao, H. Zhu, P. Sun, R. Wu, and Z. Zheng, "Simultaneous coded aperture and dictionary optimization in compressive spectral imaging via coherence minimization," *Opt. Exp.*, vol. 28, no. 18, pp. 26587–26600, 2020, doi: [10.1364/OE.396260](https://doi.org/10.1364/OE.396260).
- [35] C. Tang, G. Y. Tian, K. Li, R. Sutthaweeikul, and J. Wu, "Smart compressed sensing for online evaluation of CFRP structure integrity," *IEEE Trans. Ind. Electron.*, vol. 64, no. 12, pp. 9608–9617, Dec. 2017, doi: [10.1109/TIE.2017.2698406](https://doi.org/10.1109/TIE.2017.2698406).